doi:10.3772/j.issn.1006-6748.2014.03.001

Study on the influence of the subsurface buoy's vibration on the vector sensor due to ocean current①

Shi Junjie (师俊杰)②, Sun Dajun, Lv Yunfei, Lan Hualin, Mei Jidan
(Key Laboratory of Underwater Acoustic Technology, Underwater Acoustic Engineering College, HarBin Engineering University, Harbin 150001, P. R. China)

Abstract

Subsurface buoy systems, especially equipped with the vector sensor, have more and more extensive applications in military and civilian regions. However, their acoustic performances are constrained by the vibration resulting from the unavoidable ocean current in some degree. The influence of such vibrations is quantitatively analyzed by means of modeling the simplified models of two deployment configurations involving the positive buoyant buoy and neutral buoy system. The corresponding formulas are deduced respectively for the deployment configuration buoy systems in the motion state firstly. Then the simulation software is developed and some numerical simulations are put up via the Runge-Kutta method. The simulation results and theoretical analysis indicate that the neutral buoy will be an excellent design protocol in engineering application in comparison with the positive buoyant buoy.

Key words: subsurface buoy system, vector sensor, ocean current, neutral buoy

0 Introduction

A subsurface buoy system is an effective device to acquire the marine environmental information, such as passing-by ships and underwater moving targets of interest radiated noise, ocean noise under a variety of sea state and so on. It can work well in the harsh marine environment in the long-term, continuous and confident manner, which characterizes its automation, safety and reliability, and fruitful information. It has a broad development prospects in the field of information access about underwater target of interest and ocean noise characteristics[1]. However, with the development of vibration reduction and noise control technology, the radiated noise in the high frequency band of underwater moving target decreases greatly, which makes underwater acoustic researches shift to low frequency gradually. Also it makes the required aperture of conventional hydrophone array become larger and larger, which limits its applications in practical engineering. Fortunately, the vector sensor inspires new ideas to solve this problem. Thus, the subsurface buoy system armed with the vector sensor has got more and more development and progress[2,3].

Unlike the conventional hydrophone, the vector sensor can measure both the particle motions and pressure changes associated with the same target of interest, while the hydrophone can only measure the pressure changes. So the vector sensor can acquire more comprehensive acoustic field information, which makes it more suitable for further signal processing and sonar capability extensions[3]. Unfortunately, the vector sensor is also sensitive to attitude changes, vibrations and ocean current, even at velocities less than 50cm/s[4,5]. During the period of subsurface buoy equipped with vector sensors working in the ocean, it is inevitably influenced by the ocean current, tide and so on, which makes it produce the attitude changes involving rotation, pitch and roll. At the same time, it also causes the buoy to vibrate forward and backward, up and down randomly[1,6-8]. In addition, the flow noise arising from the ocean current over the vector sensor or its housing is often a major source of interference. All these influences are usually directly coupled to the vector sensor sensing elements, in which the acoustic information acquired by the vector sensor may be corrupted by these influence factors, and even they can't be used for further research, such as target direction of arrival (DOA) estimation, target classification and recognition and so forth[5].

① Supported by the National High Technology Research and Development Programme of China (No. 2011AA090502) and the National Defense Foundation Project (No. B2420110006).

② To whom correspondence should be addressed. E-mail: junejieshi@gmail.com

Received on Dec 19, 2012

This paper focuses on the vibration influence on the subsurface buoy introduced by the ocean current, tide, etc. In Section 0, it introduces the background and the influence factors to subsurface buoy. In Section 1, it conducts the mechanical analysis of two simplified subsurface buoy models and derives the differential equations for the buoy motions. In what follows, in Section 2 it validates the theoretical analysis in second section through numerical simulation. It is summarized in Section 3 indicating that the neutral buoy is an excellent design protocol and arranges the next work.

1 Mechanical analysis of subsurface buoy systems

The subsurface buoy system is a complex device and may have many deployment configurations. Here, two deployment configurations are discussed, which are illustrated in Fig. 1 and Fig. 2. In Fig. 1, the subsurface buoy has positive resultant force[3], i. e. the buoy gravity is smaller than its buoyance. On the other hand, the subsurface buoy in Fig. 2 may have positive, or negative even zero resultant force, among which there may exist an optimal choice, and it can mitigate the vibration arising from ocean current[9].

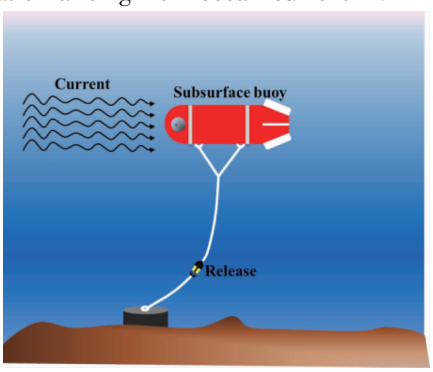

Fig. 1 Deployment configuration A

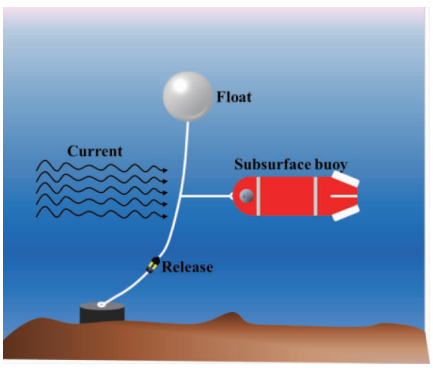

Fig. 2 Deployment configuration B

For the sake of analyzing conveniently, here it will simplify the two deployment configurations. In these simplified models, suppose all ropes are ideal and their gravities are not considered into the motion equations about the buoy. The acoustic release is neglected. In addition, the shape of the float and the subsurface buoy is omitted and are seen as particles. Moreover, the force produced by the ocean current is harmonic, i. e. $F_0 + A\cos\omega t$. Here term F_0 is the equivalent force of the initial condition, and A and ω are the force amplitude and frequency respectively. If the motion equations about the buoy constructed, the vibration influence on the subsurface buoy due to ocean current would be analyzed.

1.1 Deployment configuration A

According to the above assumptions, mechanical analysis of deployment configuration A is depicted in Fig. 3. The subsurface buoy locates at $O_1(x_0, z_0)$ initially, imposed by resultant force B between buoy gravity and its buoyance, strike force F of ocean flow and pull force P of the rope with the length of L. Owing to the impact of ocean current, it will move from $O_1(x_0, z_0)$ to $O'_1(x, z)$. Hereinafter, the relative motion equations about the buoy will be derived.

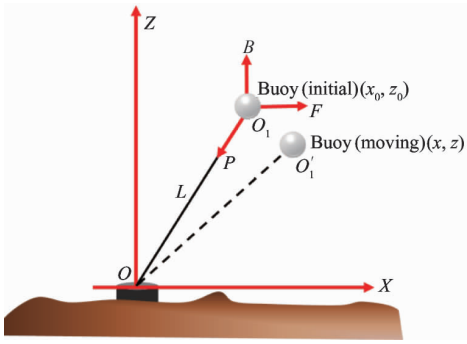

Fig. 3 Mechanical analysis of deployment configuration A

Considering the second law of Newton, the motion equations about the buoy can be achieved as follows:

$$\begin{cases} F - P\dfrac{x}{L} = m\dfrac{\mathrm{d}^2x}{\mathrm{d}t^2} \\ B - P\dfrac{z}{L} = m\dfrac{\mathrm{d}^2z}{\mathrm{d}t^2} \end{cases} \tag{1}$$

where m is the quality of the subsurface buoy. From Eq. (1), parameter P is eliminated and a first two-order differential equation about the buoy will be got:

$$mz\frac{\mathrm{d}^2x}{\mathrm{d}t^2} - mx\frac{\mathrm{d}^2z}{\mathrm{d}t^2} = Fz - Bx \tag{2}$$

On the other hand, the rope holds the length unchanged, i. e.:

$$x^2 + z^2 = x_0^2 + z_0^2 = L^2 \tag{3}$$

Differentiating Eq. (3) and a second differential equation can be expressed as

$$x\frac{\mathrm{d}^2x}{\mathrm{d}t^2} + z\frac{\mathrm{d}^2z}{\mathrm{d}t^2} = -\left(\frac{\mathrm{d}x}{\mathrm{d}t}\right)^2 - \left(\frac{\mathrm{d}z}{\mathrm{d}t}\right)^2 \tag{4}$$

Combining Eq. (2) and Eq. (4) and introducing the following notations:

$$\begin{cases} y_1 = \dfrac{\mathrm{d}^2 x}{\mathrm{d}t^2} \\ y_2 = \dfrac{\mathrm{d}^2 z}{\mathrm{d}t^2} \end{cases} \tag{5}$$

$$\begin{cases} a_{11} = mz \quad a_{12} = -mx \quad b_1 = Fz - Bx \\ a_{21} = x \quad a_{22} = z \quad b_2 = -\left(\dfrac{\mathrm{d}x}{\mathrm{d}t}\right)^2 - \left(\dfrac{\mathrm{d}z}{\mathrm{d}t}\right)^2 \end{cases} \tag{6}$$

A set of two two-order differential equations about the buoy will be attained finally:

$$\begin{bmatrix} a_{11} & a_{12} \\ a_{21} & a_{22} \end{bmatrix} \begin{bmatrix} y_1 \\ y_2 \end{bmatrix} = \begin{bmatrix} b_1 \\ b_2 \end{bmatrix} \tag{7}$$

And the following initial conditions should be satisfied:

$$\begin{cases} x(t)\big|_{t=0} = x_0 \\ \left.\dfrac{\mathrm{d}x(t)}{\mathrm{d}t}\right|_{t=0} = 0 \\ z(t)\big|_{t=0} = z_0 \\ \left.\dfrac{\mathrm{d}z(t)}{\mathrm{d}t}\right|_{t=0} = 0 \end{cases} \tag{8}$$

As can be seen from Eq. (2) and Eq. (4), the motion equations of the buoy are nonlinear and perhaps can be solved through numerical calculation method, such as the Runge-Kutta method[10]. Here Eq. (7) can make the computation convenient.

1.2 Deployment configuration B

Deployment configuration B may be a more complex configuration, but it may mitigate the vibration influence on the buoy due to the ocean current in a high degree. Mechanical analysis of the simplified model of configuration B is depicted in Fig. 4. Initially, the float locates at $O_1(x_{01}, z_{01})$, imposed by resultant force B_1 between buoy gravity and its buoyance, strike force F_1 of ocean flow and pull force P_1 of the rope with the length of L_1. Due to the impact of ocean current, it will move from $O_1(x_{01}, z_{01})$ to $O'_1(x_1, z_1)$. The subsurface buoy initially rests at $O_2(x_{02}, z_{02})$, with the corresponding parameters B_2, F_2, P_2 and L_2 respectively and move to $O'_2(x_2, z_2)$ in the same way. In addition, the connection knot of the three ropes is at the position of $O_3(x_{03}, z_{03})$ at the beginning, and can move from $O_3(x_{03}, z_{03})$ to $O'_3(x_3, z_3)$. Moreover, the length from the connection knot to the origin is L_3.

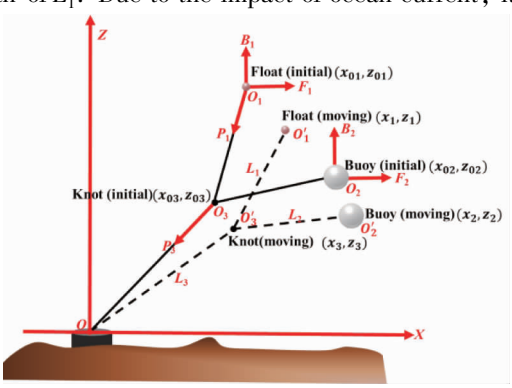

Fig. 4 Mechanical analysis of deployment configuration B

Deducing in the same way as in Section 1.1, the motion equations about the float, the buoy and the connection knot can be achieved as follows:

$$m_1(z_1 - z_3)\frac{\mathrm{d}^2 x_1}{\mathrm{d}t^2} - m_1(x_1 - x_3)\frac{\mathrm{d}^2 z_1}{\mathrm{d}t^2} = F_1(z_1 - z_3) - B_1(x_1 - x_3) \tag{9}$$

$$m_2(z_2 - z_3)\frac{\mathrm{d}^2 x_2}{\mathrm{d}t^2} - m_2(x_2 - x_3)\frac{\mathrm{d}^2 z_2}{\mathrm{d}t^2} = F_2(z_2 - z_3) - B_2(x_2 - x_3) \tag{10}$$

$$m_1 z_3 \frac{\mathrm{d}^2 x_1}{\mathrm{d}t^2} - m_1 x_3 \frac{\mathrm{d}^2 z_1}{\mathrm{d}t^2} + m_2 z_3 \frac{\mathrm{d}^2 x_2}{\mathrm{d}t^2} - m_2 x_3 \frac{\mathrm{d}^2 z_2}{\mathrm{d}t^2} = (F_1 + F_2) z_3 - (B_1 + B_2) x_3 \tag{11}$$

where m_1 and m_2 are the quality of the float and the subsurface buoy respectively. Besides, the three ropes hold their length unchanged, i.e.:

$$(x_{01} - x_{03})^2 + (z_{01} - z_{03})^2 = (x_1 - x_3)^2 + (z_1 - z_3)^2 = L_1^2 \tag{12}$$

$$(x_{02} - x_{03})^2 + (z_{02} - z_{03})^2 = (x_2 - x_3)^2 + (z_2 - z_3)^2 = L_2^2 \tag{13}$$

$$x_{03}^2 + z_{03}^2 = x_3^2 + z_3^2 = L_3^2 \tag{14}$$

Differentiating the equations from Eq. (12) to Eq. (14) and the two-order differential equations can be expressed as:

$$(x_1 - x_3)\frac{\mathrm{d}^2 x_1}{\mathrm{d}t^2} + (z_1 - z_3)\frac{\mathrm{d}^2 z_1}{\mathrm{d}t^2} - (x_1 - x_3)\frac{\mathrm{d}^2 x_3}{\mathrm{d}t^2} - (z_1 - z_3)\frac{\mathrm{d}^2 z_3}{\mathrm{d}t^2} = -\left(\frac{\mathrm{d}x_1}{\mathrm{d}t} - \frac{\mathrm{d}x_3}{\mathrm{d}t}\right)^2 - \left(\frac{\mathrm{d}z_1}{\mathrm{d}t} - \frac{\mathrm{d}z_3}{\mathrm{d}t}\right)^2 \tag{15}$$

$$(x_2 - x_3)\frac{\mathrm{d}^2 x_2}{\mathrm{d}t^2} + (z_2 - z_3)\frac{\mathrm{d}^2 z_2}{\mathrm{d}t^2} - (x_2 - x_3)\frac{\mathrm{d}^2 x_3}{\mathrm{d}t^2} - (z_2 - z_3)\frac{\mathrm{d}^2 z_3}{\mathrm{d}t^2} = -\left(\frac{\mathrm{d}x_2}{\mathrm{d}t} - \frac{\mathrm{d}x_3}{\mathrm{d}t}\right)^2 - \left(\frac{\mathrm{d}z_2}{\mathrm{d}t} - \frac{\mathrm{d}z_3}{\mathrm{d}t}\right)^2 \tag{16}$$

$$x_3 \frac{\mathrm{d}^2 x_3}{\mathrm{d}t^2} + z_3 \frac{\mathrm{d}^2 z_3}{\mathrm{d}t^2} = -\left(\frac{\mathrm{d}x_3}{\mathrm{d}t}\right)^2 - \left(\frac{\mathrm{d}z_3}{\mathrm{d}t}\right)^2 \tag{17}$$

Introducing the following notations:

$$\begin{cases} y_1 = \dfrac{\mathrm{d}^2 x_1}{\mathrm{d}t^2} \quad y_2 = \dfrac{\mathrm{d}^2 z_1}{\mathrm{d}t^2} \\ y_3 = \dfrac{\mathrm{d}^2 x_2}{\mathrm{d}t^2} \quad y_4 = \dfrac{\mathrm{d}^2 z_2}{\mathrm{d}t^2} \\ y_5 = \dfrac{\mathrm{d}^2 x_5}{\mathrm{d}t^2} \quad y_6 = \dfrac{\mathrm{d}^2 z_3}{\mathrm{d}t^2} \end{cases} \tag{18}$$

$$\begin{cases} a_{11} = m_1(z_1 - z_3),\ a_{12} = -m_1(x_1 - d_3), \\ b_1 = F_1(z_1 - z_3) - B_1(x_1 - x_3) \\ a_{23} = m_2(z_2 - z_3),\ a_{24} = -m_2(x_2 - d_3), \\ b_2 = F_2(z_2 - z_3) - B_2(x_2 - x_3) \\ a_{31} = m_1 z_3,\ a_{32} = -m_1 x_3,\ a_{33} = m_3 z_3, \\ a_{34} = -m_2 x_3,\ b_3 = (F_1 + F_2)z_3 - (B_1 + B_2)x_3 \\ a_{41} = x_1 - x_3,\ a_{42} = z_1 - z_3, \\ b_4 = -\left(\frac{dx_1}{dt} - \frac{dx_3}{dt}\right)^2 - \left(\frac{dz_1}{dt} - \frac{dz_3}{dt}\right)^2 \\ a_{53} = x_2 - x_3,\ a_{54} = z_2 - z_3, \\ b_5 = -\left(\frac{dx_2}{dt} - \frac{dx_3}{dt}\right)^2 - \left(\frac{dz_2}{dt} - \frac{dz_3}{dt}\right)^2 \\ a_{65} = x_3,\ a_{66} = z_3,\ b_6 = -\left(\frac{dx_3}{dt}\right)^2 - \left(\frac{dz_3}{dt}\right)^2 \end{cases} \tag{19}$$

A set of six two-order differential equations about the buoy will be obtained finally, which are also nonlinear equations.

$$\begin{bmatrix} a_{11} & a_{12} & 0 & 0 & 0 & 0 \\ 0 & 0 & a_{23} & a_{24} & 0 & 0 \\ a_{31} & a_{32} & a_{33} & a_{34} & 0 & 0 \\ a_{41} & a_{42} & 0 & 0 & -a_{41} & -a_{42} \\ 0 & 0 & a_{53} & a_{54} & -a_{53} & -a_{54} \\ 0 & 0 & 0 & 0 & a_{65} & a_{66} \end{bmatrix} \begin{bmatrix} y_1 \\ y_2 \\ y_3 \\ y_4 \\ y_5 \\ y_6 \end{bmatrix} = \begin{bmatrix} b_1 \\ b_2 \\ b_3 \\ b_4 \\ b_5 \\ b_6 \end{bmatrix} \tag{20}$$

And the following initial conditions should be satisfied:

$$\begin{cases} x_1(t)\big|_{t=0} = x_{01} \\ \left.\frac{dx_1(t)}{dt}\right|_{t=0} = 0 \\ z_1(t)\big|_{t=0} = z_{01} \\ \left.\frac{dz_1(t)}{dt}\right|_{t=0} = 0 \\ x_2(t)\big|_{t=0} = x_{02} \\ \left.\frac{dx_2(t)}{dt}\right|_{t=0} = 0 \\ z_2(t)\big|_{t=0} = z_{02} \\ \left.\frac{dz_2(t)}{dt}\right|_{t=0} = 0 \\ x_3(t)\big|_{t=0} = x_{03} \\ \left.\frac{dx_3(t)}{dt}\right|_{t=0} = 0 \\ z_3(t)\big|_{t=0} = z_{03} \\ \left.\frac{dz_3(t)}{dt}\right|_{t=0} = 0 \end{cases} \tag{21}$$

2 Numerical simulation and analysis

Here, numerical simulation for configuration A and B is proceeded respectively and influence of the subsurface buoy resulting from the ocean current is studied. First of all, the simulation software is developed. Then the numerical simulations are conducted by the Runge-Kutta method[10]. For the deployment configuration A, the simulations are divided into two cases. On one hand, resultant force B between the buoy gravity and its buoyance is changed with some fixed strike force F of ocean flow. On the other hand, strike force F of ocean current is changed with constant resultant force B. For configuration B, the condition of resultant force B is studied under which it can make the vibration imposed upon the buoy the smallest.

2.1 Simulation software development

The simulation software is developed in C language[11], and the major interfaces are listed in Fig. 5 and Fig. 6, in which they are the software simulation interfaces for configuration A and B respectively. After numerical computations, the resultant data is stored as a MAT file, which can be read, analyzed and depicted in MATLAB platform.

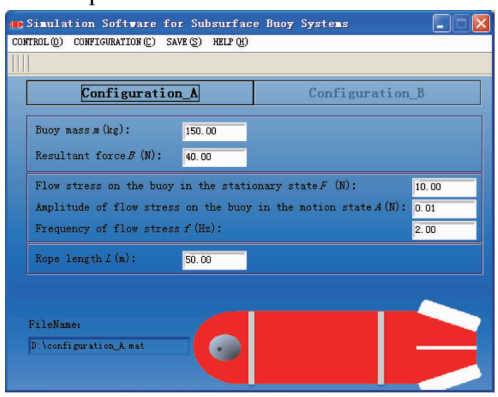

Fig. 5 Software simulation interface for configuration A

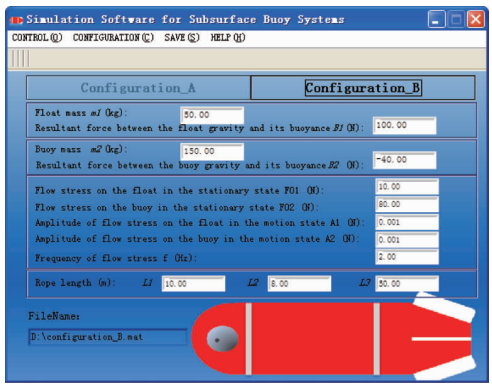

Fig. 6 Software simulation interface for configuration B

2.2 Simulation results for configuration A

As stated above, the simulation parameters for configuration A are listed in Table 1, where amplitude A of flow stress on the buoy in the motion state is equivalent to -40dB.

Table1 Simulation parameters for configuration A

Parameters	Case 1	Case 2
Buoy mass m (kg)	150	150
Flow stress on the buoy in the stationary state F (N)	10	40 ~ 60
Amplitude of flow stress on the buoy in the motion state A (N)	0.01	0.01
Frequency of flow stress f (Hz)	2 ~ 10	2 ~ 10
Rope length L (m)	50	50
Resultant force B (N)	40 ~ 60	80

The simulation results are illustrated in Fig. 7 ~ Fig. 10. Fig. 7and Fig. 8 are for case one, of which Fig. 7 is the vibration force arising from ocean flow on the buoy in z direction, Fig. 8 in x direction. Fig. 9 and Fig. 10 are the results for case two. Among these figures, the x axis denotes frequency of flow stress and y coordinate is resultant force B or flow stress on the buoy in the stationary state respectively. The color indicates the vibration force on the buoy with the unit of decibel. As can be seen from Fig. 5 to Fig. 8, compared with flow stress on the buoy in the stationary state, the larger the buoyance of the buoy is, the smaller the vibration force on the buoy in z direction is, but the larger in x direction. This can be interpreted from Eq. (3). According to Eq. (3), we can obtain the following expression:

$$x\frac{\mathrm{d}x}{\mathrm{d}t} + z\frac{\mathrm{d}z}{\mathrm{d}t} = 0 \tag{22}$$

Eq. (22) can be transformed further as:

$$\left|\frac{v_x}{v_z}\right| = \left|\frac{z}{x}\right| \tag{23}$$

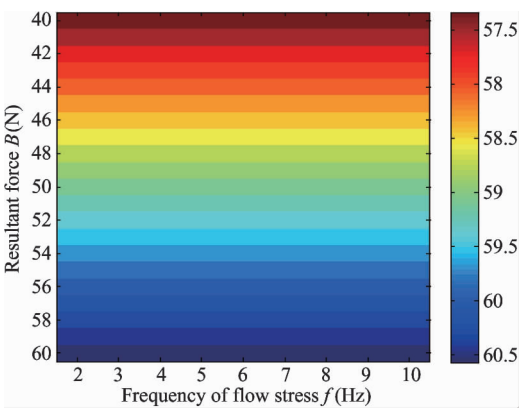

Fig. 7 Vibration force on the buoy in z direction for case A

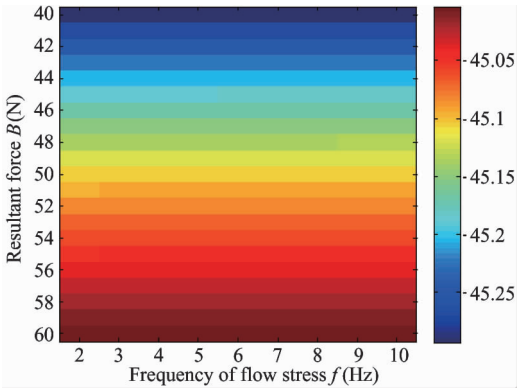

Fig. 8 Vibration force on the buoy in x direction for case A

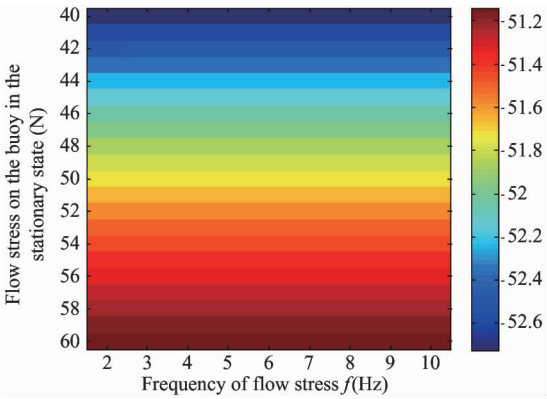

Fig. 9 Vibration force on the buoy in z direction for case B

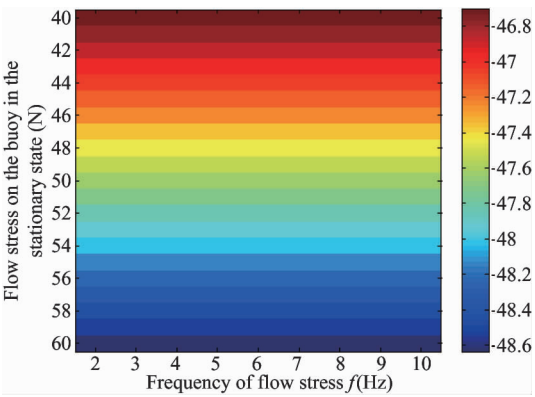

Fig. 10 Vibration force on the buoy in x direction for case B

From Eq. (23), it is concluded that the smaller the buoy coordinate x_0 in the initial state is, the smaller the vibration velocity in z direction is. This is consistent to the larger buoyance of the buoy. In addition, we can summarize from these figures that the vibration forces in z and x directions are both smaller than the input of ocean current, which means that deployment configuration A has damping nature just like a filter. But the filter performance is not outstanding.

2.3 Simulation results for configuration B

Compared with deployment configuration A, con-

figuration B may have more parameters to determine its acoustic characteristics. All the simulation parameters for configuration B are tabled in Table 2, where amplitude A_1 and A_2 of flow stress on the float and buoy in the motion state is equivalent to -60dB and -40dB respectively.

Table 2 Simulation parameters for configuration B

Parameters	Configuration B
Float mass m_1 (kg)	50
Buoy mass m_2 (kg)	150
Resultant force between the float gravity and its buoyance B_1 (N)	100
Resultant force between the buoy gravity and its buoyance B_2 (N)	$-40 \sim 40$
Flow stress on the float in the stationary state F_{01} (N)	10
Flow stress on the buoy in the stationary state F_{02} (N)	80
Amplitude of flow stress on the float in the motion state A_1 (N)	0.001
Amplitude of flow stress on the buoy in the motion state A_2 (N)	0.01
Rope length L_1 (m)	10
Rope length L_2 (m)	8
Rope length L_3 (m)	50
Frequency of flow stress f (Hz)	$2 \sim 10$

Fig. 11 and Fig. 12 give the simulation results about the vibration force on the buoy in z and x directions for deployment configuration B. In both figures, the x coordinate is the frequency of flow stress and y axis is the resultant force B_2. The color still represents the vibration force on the buoy with the unit of decibel. As can be concluded from Fig. 11 and Fig. 12, the more resultant force B_2 approaches to zero, the smaller the vibration force will be on the buoy in both z and x directions. As can be seen from Fig. 13, the mitigation

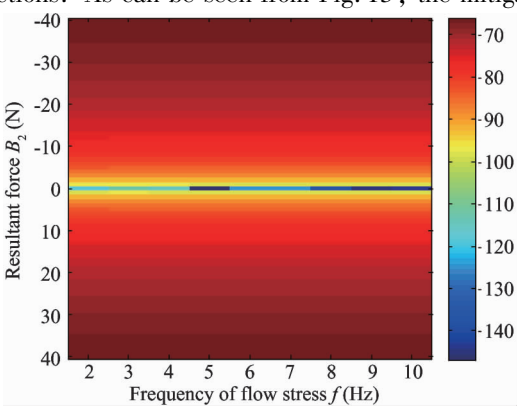

Fig. 11 Vibration force on the buoy in the z direction for configuration B

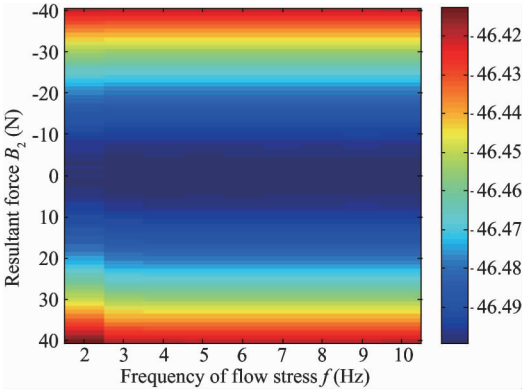

Fig. 12 Vibration force on the buoy in the x direction for configuration B

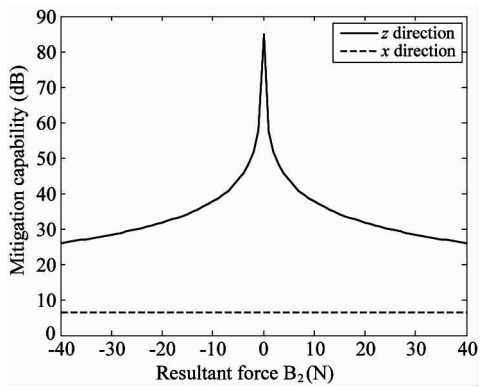

Fig. 13 Mitigation capability to ocean current influence

capability to ocean current influence is nearly 90dB in the z direction for neutral buoy in comparison with about 20dB for positive buoyant buoy depicted in Fig. 7 and Fig. 9. Here, we can think configuration B as a cascade structure of two configurations A. Its filter characteristics can have a great deal improvement, especially in the z direction. In other words, deployment configuration B may be a better choice in practice. In this condition, the signal of interest recorded by the vector sensor especially in the z direction will not be corrupted by the vibrations due to the ocean current influence. And it will improve the signal processing performance through long time integration to extend sonar capability[3].

3 Conclusion and further work

This article focuses on the vibration influence on the subsurface buoy resulting from the ocean current. It firstly derives the motion equations of two simplified deployment configurations of the subsurface buoy system. Then it analyzes the constructed differential models through numerical calculation via the Runge-Kutta algorithm. The numerical simulation results and theoretical analysis indicate that:

(1) For configuration A, the larger the buoyance of the buoy is, the smaller the vibration force on the buoy is in the z direction;

(2) For configuration B, the more resultant force of the buoy approaches to zero, the smaller the vibration force is on the buoy in both z and x directions;

(3) In practice, deployment configuration B may be an advantageous choice in engineering application, which is propitious to improve the post signal processing performance to extend the sonar detection capability.

The work in this paper is very meaningful for designing the subsurface buoy. However, the subsurface buoy system is a complicated engineering project, which is needed to think about the influence of the buoy's shape and material, installation, and flow noise on vector sensor. Here is the next work to do about the ocean current and flow noise:

(1) Vibration analysis in the condition of quasi-real ocean current is done, using software CFD;

(2) Flow noise analysis for deployment configuration B.

References

[1] Sun Y L, Zhu L J, Na J, et al. Buoyed under water noise monitor system. *Journal of test and measurement technology*, 2002, 16: 505-508

[2] Luo C. Research on DOA estimation based on vector sensor array: [Master dissertation]. Xi'An: Northwest Industrial University, 2006. 1-2

[3] Shi J J. Modelling and experiment studies on very low frequency vector acoustic field based on subsurface buoy: [Ph. D dissertation]. HarBin: HarBin Enginering University, 2011. 15

[4] Lauchle G C, McEachern J F, Jones A R, et al. Flow induced noise on pressure gradient hydrophones. In: Proceedings of American Institute of Physics Conference on Acoustic Particle Velocity Sensors: Design, Performance, and Applications, Mystic Connecticut, USA, 1995. 202-225

[5] Zou N, Arye N. Acoustic vector-sensor beamforming in the presence of flow noise. In: Proceedings of IEEE International Conference on Acoustics, Speech and Signal Processing, Prague Czech Republic, 2011. 2652-2655

[6] Walter P, Donald B P. Compliant ocean wave mitigation device and method to allow underwater sound detection with oceanographic buoy moorings. US patent: 20100246331A1, 2010

[7] James F M, James A M, John J, et al. ARAP - deep ocean vector sensor research array. In: Proceeding of IEEE Oceans Conference, Boston, USA, 2006. 1-5

[8] Aaron T, Jeff S, Pam S, el al. Tracking sperm whales with a towed acoustic vector sensor. *J Acoust Soc Am*, 2010, 128(5): 2681-2694

[9] V. A. S. Vector Acoustics of the Ocean. Vladivostok: Dalnauka, 2006. 45-49

[10] Lv T F, Kang Z M, Fang X N. Numeric Computational Method. Beijing: Tsinghua University Publishers, 2008. 278-283

[11] Wang J X, Sui M L. LabWindowns/CVI Vitual Instrument Measurement Technology and Engineering Application. Beijing: Chemical Industry Publisher, 2011. 48-50, 289-320

Shi Junjie, born in 1980. He received his Ph. D degree in underwater acoustic engineering of HarBin Engineering University in 2011. He also received his B. S. degree from HarBin Engineering University in 2005. His research interests include acoustic field calculation & analysis, and signal-processing.